Proceedings of the
Annual Stability Conference
Structural Stability Research Council
Atlanta, Georgia, April 21-24, 2026

Numerical investigation on dynamic buckling behavior of thin-walled cylindrical storage tanks subjected to seismic excitations

Shafqat Ullah[1], Iraj H. P. Mamaghani[2]

Abstract
In recent decades, numerous large-scale cylindrical storage tanks have been constructed worldwide to store petrochemicals, water, and liquefied natural gas (LNG). Due to their thin-walled shell configuration, these tanks are highly susceptible to local and global buckling under seismic loading, with potential consequences including severe economic losses, environmental damage, and risks to human life. Traditional analytical approaches rely on simplified assumptions and therefore cannot accurately capture the nonlinear seismic behavior and complex fluid–structure interaction (FSI) of liquid-filled tanks. Consequently, high-fidelity finite element modeling (FEM) is required to realistically simulate FSI effects, including hydrodynamic pressure distribution, nonlinear sloshing behavior, and variations in hydrodynamic stresses along the tank height.

This study presents an FEM–based approach to investigate the dynamic buckling behavior of cylindrical storage tanks subjected to steady-state sinusoidal excitation. The numerical model is first validated against experimental results from the literature, followed by a parametric investigation to evaluate the influence of excitation intensity on the dynamic buckling response. The comparisons demonstrate good agreement with previously reported experimental and numerical findings. The finite element (FE) model predicts a peak shear force of 44.27 kN, compared with 47.30 kN measured experimentally, yielding a discrepancy of 6.41%. Similarly, the predicted bending moment of 57.90 MN-mm compares well with the experimental value of 61.37 MN-mm, resulting in a difference of 6.19%. The parametric results indicate that shear force, bending moment, and von Mises stress are highly sensitive to changes in input seismic excitation. At an excitation level of 2.7g, the maximum shear force and bending moment were 58.53 kN and 62.94 MN-mm, respectively. When the excitation increased to 3.2g, the shear force and bending moment reached to 67.91 kN and 78.00 MN-mm, corresponding to increases of approximately 16.0% and 23.9%, respectively. These results demonstrate that the dynamic response of the storage tank intensifies significantly with increasing seismic acceleration.

Keywords: Cylindrical storage tanks, local buckling, hydrodynamic pressure, base shear, bending moment, seismic excitation, ABAQUS.

1. Introduction

Cylindrical steel tanks are a cornerstone of industrial storage for hazardous liquids, including oil, petrochemicals, and LNG. Experience from several strong earthquakes has exposed significant

[1] PhD student, University of North Dakota, <shafqat.ullah@und.edu>
[2] Professor, University of North Dakota, <iraj.mamaghani@und.edu>

gaps in their seismic reliability. Post-earthquake reconnaissance consistently documented characteristic instabilities and connection failures, including lower-shell "elephant-foot" and diamond-shaped buckling, roof damage, base-plate and anchorage failures, leg instability in supported storage tanks, and nozzle damage. Fig. 1(a–c) illustrates the elephant ' s-foot, diamond-shaped, and secondary buckling modes, respectively (Buratti and Tavano 2014; Rammerstorfer et al. 1990). Several researchers have continued their efforts in understanding the dynamic behavior of cylindrical storage tanks using experimental, numerical and analytical approach. For instance, Chen et al. (2007) analyzed the sloshing response of cylindrical steel tanks subjected to harmonic base excitations, integrating laboratory-scale testing with finite element simulations to validate

(a) (b) (c)

Figure 1. Buckling in steel Tanks (a). Elephant's foot Buckling (b). Diamond shaped Buckling and (c). Secondary Buckling (Buratti and Tavano, 2014; Rammerstorfer et al. 1990)

hydrodynamic pressure distributions and free-surface behavior. Sobhan et al. (2017) evaluated the dynamic buckling performance of anchored steel tanks under combined horizontal–vertical ground motions, employing nonlinear static pushover and incremental dynamic analysis (IDA) to quantify instability thresholds and demand–capacity relationships. Jing et al. (2022) investigated the seismic behavior of liquid storage tanks by explicitly accounting for both FSI and soil–structure interaction (SSI) effects. Their study provided a comprehensive assessment of how the coupled interactions between the contained fluid, tank structure, and supporting soil influence the dynamic response, stress distribution, and overall seismic performance of the system.
Recently, Ulloa-Rojas et al. (2024) employed a capacity spectrum method to assess local instability in anchored and unanchored steel storage tanks, quantifying the influence of soil parameters across a suite of recorded earthquakes. The study estimated the critical peak ground acceleration (PGA_{cr}) associated with the onset of shell buckling for each configuration. Other researchers, such as Bakalis et al. (2017), developed a 3D surrogate modeling framework for the seismic assessment of cylindrical storage tanks, with the focus on squat unanchored tank systems. The authors performed a global sensitivity analysis to identify how key modeling parameters govern the predicted seismic response of the proposed tank models.

A recent study of Bakalis and Karamanos (2021) investigated the uplift mechanics of unanchored cylindrical steel tanks subjected to lateral seismic excitation. The authors characterized the uplift phenomenon through combined numerical–analytical evaluation and proposed an analytical formulation that efficiently captures the uplift response of the shell–base system. Ozdemir et al. (2010) conducted nonlinear dynamic analyses of both anchored and unanchored cylindrical steel storage tanks, explicitly incorporating FSI effects through finite element simulations accompanied by laboratory experiments. The study evaluated the time histories of sloshing response, base-plate uplift, and tank wall stresses, and compared the numerical predictions with experimental

measurements, demonstrating strong agreement and validating the reliability of the proposed FE modeling approach. Lyu et al. (2020) proposed a simplified approach for the seismic design of above-ground storage tanks that explicitly accounts for soil–structure and fluid–structure coupling. Their results show that incorporating these interactions increases key seismic demand measures, particularly base shear, overturning moment, and sloshing wave height relative to models that neglect SSI/FSI effects. Bektaş and Aktaş (2023) examined the seismic vulnerability of unanchored cylindrical steel tanks with emphasis on elephant-foot buckling. Using IDA approach, they evaluated the response both with and without material-property uncertainty, and developed fragility curves quantifying the probability of buckling-induced failure across intensity levels. Maekawa (2012) investigated the dynamic behavior of cylindrical aluminum storage tanks subjected to sinusoidal input waves. The base shear, overturning moment, and buckling capacity of the tank were computed and validated against experimental results, demonstrating close correlation between the analytical and experimental responses.

Ullah and Mamaghani (2025) performed a comprehensive FEA to examine the dynamic buckling response of cylindrical steel storage tanks of varying height-to-diameter ratios under seismic loading. The authors investigated stress concentrations, deformation response, and the time history of hydrodynamic pressure. The results show that impulsive hydrodynamic pressures dominate at the tank base, while free-surface sloshing induces convective pressures that control the upper-wall demand and may cause local damage. The investigations demonstrate that explicitly modeling FSI has a pronounced influence on the seismic response of liquid storage tanks. When FSI effects are considered, the resulting hydrodynamic pressure distribution and sloshing wave heights differ substantially from those predicted by linear or simplified analysis procedures, indicating that such simplified approaches may not capture the true demand on the tank system.

In summary, the reviewed studies highlight the necessity of performing detailed nonlinear dynamic analyses to accurately assess buckling behavior in liquid storage tanks, with particular emphasis on fluid-structure coupling effects. Furthermore, a comprehensive investigation of material parameters and the influence of input-motion frequency content is essential for reliably characterizing the seismic response of these systems. This study investigates the nonlinear dynamic response of an aluminum cylindrical storage tank subjected to steady-state sinusoidal base excitations. First, the FE model is validated by comparing its predictions with previously published experimental and numerical results. Subsequently, a parametric analysis is conducted on aluminum cylindrical tanks subjected to three different steady-state sinusoidal input excitations. The corresponding deformation response, stress distribution, hydrodynamic pressure, base shear, and overturning bending moment are evaluated and compared to examine the influence of the imposed sinusoidal excitations on tank behavior.

2. Finite Element Modeling (FEM)

This study employs high-fidelity FEA in Abaqus with particular emphasize on the interaction between the contained liquid and the tank wall is captured with the coupled acoustic–structure (CAS) approach, wherein an acoustic fluid domain is fully coupled to the structural shell. This approach is widely used to accurately capture the complex fluid-structure interaction (FSI) in liquid-containing storage tanks (Rawat et al. 2019; Ullah and Mamaghani 2025). In this approach, the liquid is idealized as an inviscid acoustic medium, allowing efficient computation of hydrodynamic pressure and sloshing modes at the fluid–structure interface while maintaining good

computational efficiency. The CAS formulation is numerically simple and stable because the liquid is treated as an acoustic (pressure-only) medium with no material advection, thereby avoiding mesh distortion and remeshing while retaining accurate small-amplitude pressure and sloshing predictions (Rawat et al. 2019; Ullah and Mamaghani 2025). Details on the CAS formulation for capturing complex FSI effects, as well as its application to a wide range of engineering problems, are well documented in the literature (Dhulipala et al. 2022; Rawat et al. 2019, 2020; Ullah and Mamaghani 2025, 2026; Zhao et al. 2026) . The material and geometric properties of the aluminum tank and liquid contents are discussed in the next sections.

2.1 Geometric Configurations and Material Properties

A cylindrical aluminum alloy tank (A5052), as reported in (Maekawa 2012), is selected for the dynamic buckling analysis subjected to steady-state sinusoidal wave motion. The tank features a uniform wall thickness of 1 mm, a height-to-radius (H/R) ratio of 2.67, and a radius-to-thickness (R/t) ratio of 450, representing a thin-walled storage configuration. The geometric configuration and key components of the actual tank model (Maekawa 2012), and overall assembly of the FE model are illustrated in Fig. 2 (a) and (b), respectively, providing a detailed representation of the tank's structural features. The yield strength and ultimate strength of the aluminum cylinder are taken as 193 MPa and 255 MPa, respectively. The material properties of the aluminum storage tank and the contained liquid are summarized in Table 1, providing the necessary input material parameters for the numerical simulation.

Table 1. Material properties of the aluminum Tank1(A5052)

Materials	Young's modulus (Gpa)	Bulk modulus (Gpa)	Poisson's ratio (v)	Density (kg/m^3)
Cylindrical Tank	69.42	–	0.33	2,680
Steel (Flange and Platform)	203.00	–	0.30	7,800
Top plate (polycarbonate)	1.96	–	0.30	11,900
Liquid content	–	2.20	–	1,000

Source: data from (Ullah and Mamaghani 2026)

2.2 Meshing

The cylindrical aluminum tank is discretized using four-node doubly curved shell elements (S4R) with reduced integration, while the contained liquid domain is represented by eight-node acoustic brick elements (C3D8R) incorporating reduced integration and hourglass control. The 3D meshing of the aluminum cylindrical tank is illustrated in Fig. 2 (c). Two different mesh sizes, 71 mm and 60 mm, are adopted to evaluate mesh sensitivity and its influence on various parameters including base shear and bending moment. Based on this assessment, a mesh size of 60 mm is selected for the final analysis, and the corresponding responses in terms of base shear and bending moment are evaluated and compared with previously reported experimental results in the literature.

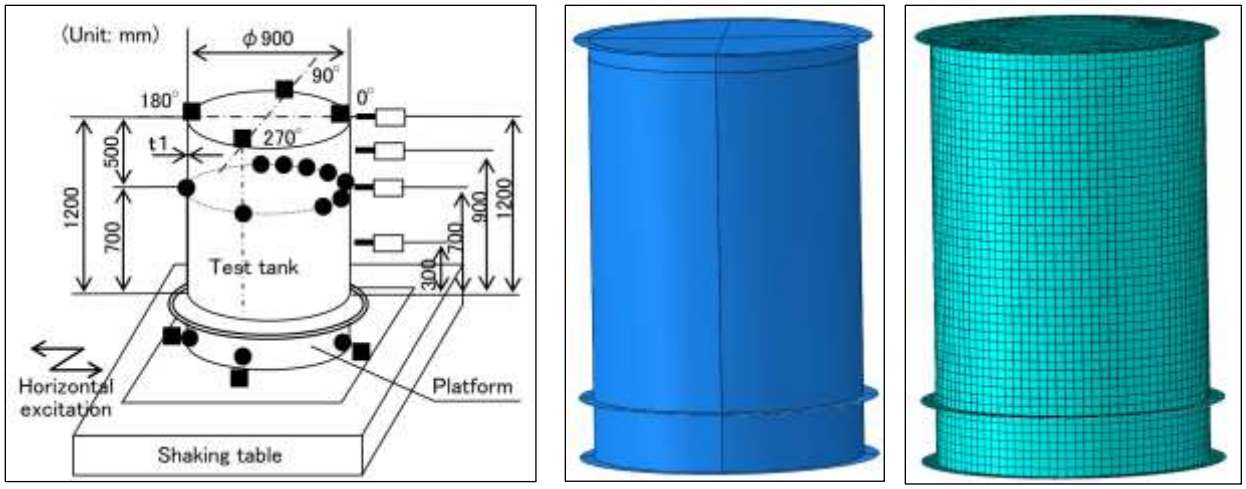

(a) (b) (c)

Figure 2 (a). Shape and dimension of different parts of the actual tank. [Reprinted from Maekawa (2012), under Creative Commons-BY-4.0 license (https://creativecommons.org/licenses/by/4.0/).]
(b). FE model and (c). 3D meshing of the Tank

2.3 Loading and Boundary Conditions

To accurately capture the dynamic buckling response of the storage tank, the loading sequence is applied in two steps. In Step 1, a nonlinear static analysis is performed by applying gravity loads over a duration of 1 second to establish the initial stress state. In Step 2, a dynamic explicit analysis is conducted over 3 seconds to simulate the tank's response under seismic excitation. A steady-state sinusoidal time-history excitation was applied in the horizontal direction as illustrated in Fig. 3. All degrees of freedom (DOFs) were fixed, except for horizontal translation, along which the excitation was applied.

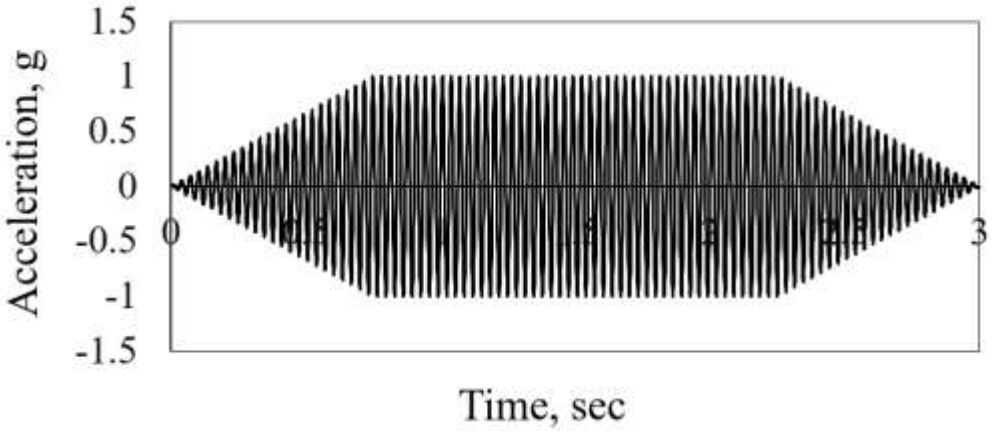

Figure 3. Time history of input waveform [reproduced from Maekawa et al. 2007]

3. Results and Discussion

3.1 Validation of FEM

To ensure the accuracy and robustness of the finite element (FE) model, a validation study (Ullah and Mamaghani 2026) is first carried out by comparing the simulated responses with available experimental data and benchmark numerical studies in the literature (Maekawa 2012; Maekawa et

al. 2007), focusing on key global response parameters including shear force and bending moment. The comparison of numerical and experimental results demonstrates strong agreement. The numerical study conducted by Ullah and Mamaghani (2026) predicted a maximum shear force of 44.27 kN, while experimental tests conducted by Maekawa et al. (2007) recorded a maximum shear force of 47.30 kN, resulting in a minor discrepancy of 6.41%. Similarly, the experimental bending moment reached 61.37 MN-mm, whereas the FE model predicted 57.90 MN-mm, corresponding to a disparity of 6.19%. Fig. 4(a) and Fig. 4(b) present the deformation responses obtained from the numerical simulation and the experimental tests, respectively. In both cases, similar deformation patterns are observed, with pronounced displacement localization concentrated near the base of the specimen. The results indicate a progressive concentration of maximum in-plane principal strain along the lower shell region as the step time increases.

Table 2. Comparisons of the dynamic buckling test and numerical results (Ullah and Mamaghani 2026)

	Method of Analysis		
Parameters	Test results (Maekawa et al. 2007)	Numerical study (Maekawa, 2012)	Current study (FEA)
Shear force (kN)	47.30	59.40	44.27
Bending moment (MN-mm)	61.80	67.70	57.79

The strain contours from 0.7 to 2.3 seconds demonstrate a continuous increase in strain demand, highlighting the development of localized deformation and the onset of potential instability near the tank base. The evolution of the maximum in-plane principal strains at different time steps are illustrated in Fig. 5. The overall comparison of the base shear and bending moment obtained from the FE analysis and the experimental tests is presented in Table 2.

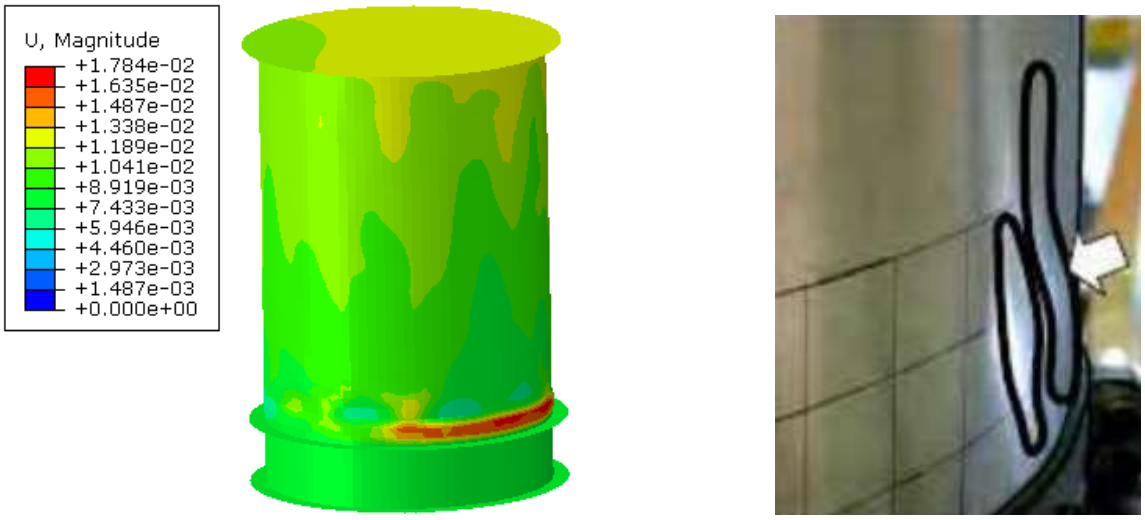

(a) (b)

Figure 4. Deformation response of the aluminum tank (a). Present study – FEA and (b). Experimental observation. [Reprinted from (Maekawa 2012), under Creative Commons-BY-4.0 license (https://creativecommons.org/licenses/by/4.0/).]

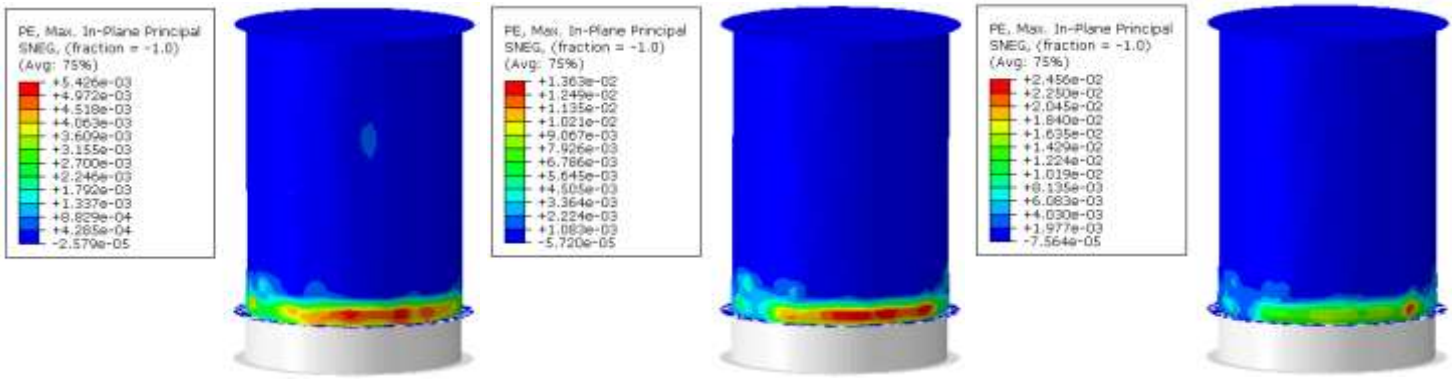

step time: 0.7 sec step time: 1.0 sec step time: 2.3 sec

Figure 5. Evolution of maximum in-plane principal strain at different time steps

3.2 Results from Parametric Analysis

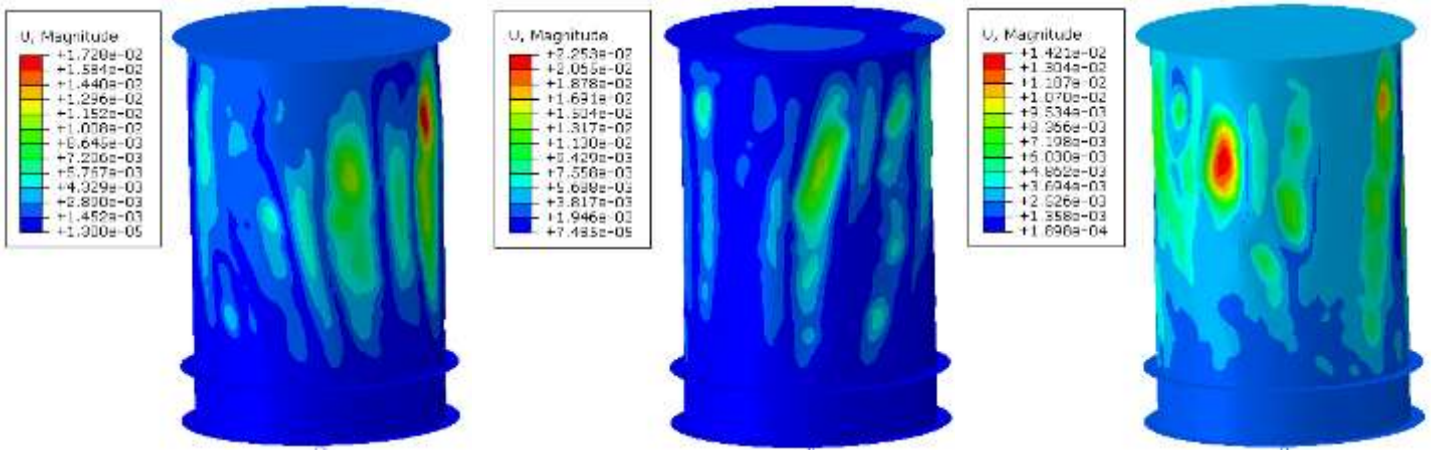

(a). step time = 0.5 sec (b). step time = 1.0 sec (c). step time = 1.4 sec

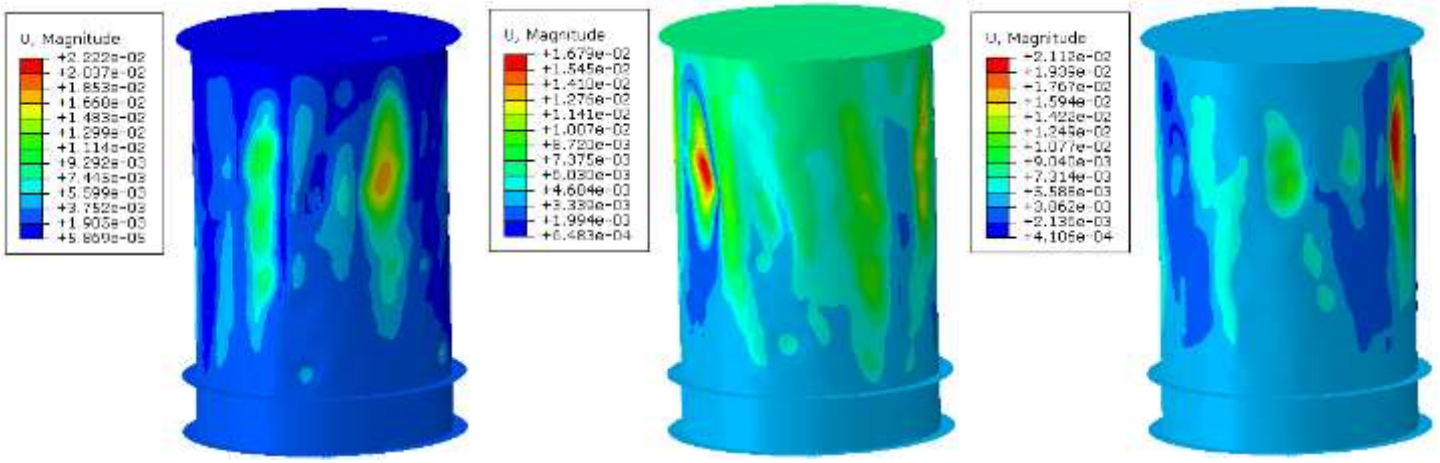

(d). step time = 2.0 sec (e). step time = 2.5 sec (f). step time = 2.7 sec

Figure 6. Deformation contour at different step time (input excitation = 2.7*g*)

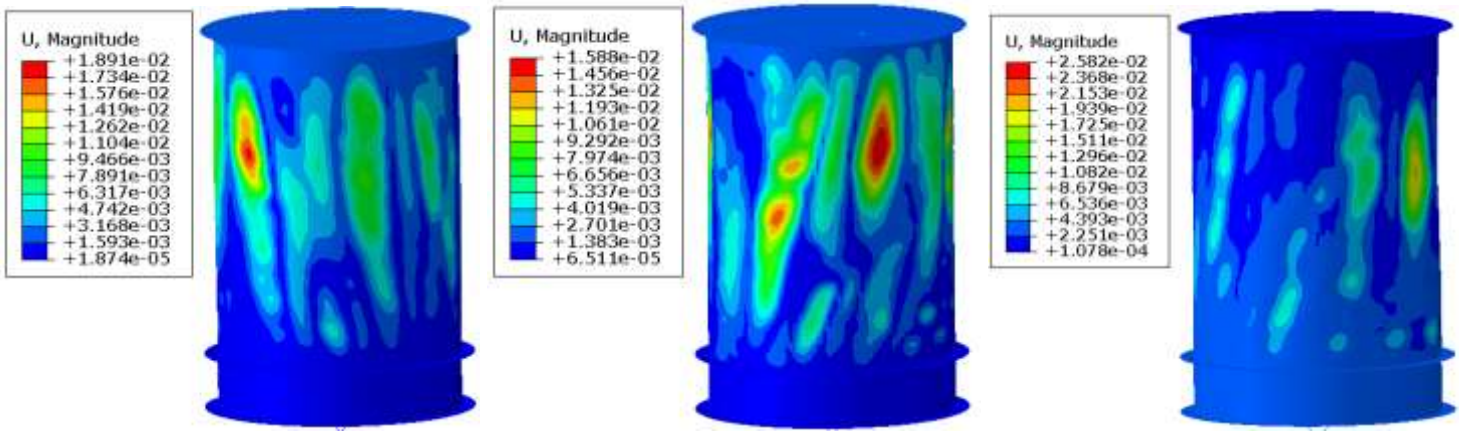

(a). step time = 0.5 sec (b). step time = 1.0 sec (c). step time = 2.0 sec

Figure 7. Deformation contour at different step time (input excitation = 3.0*g*)

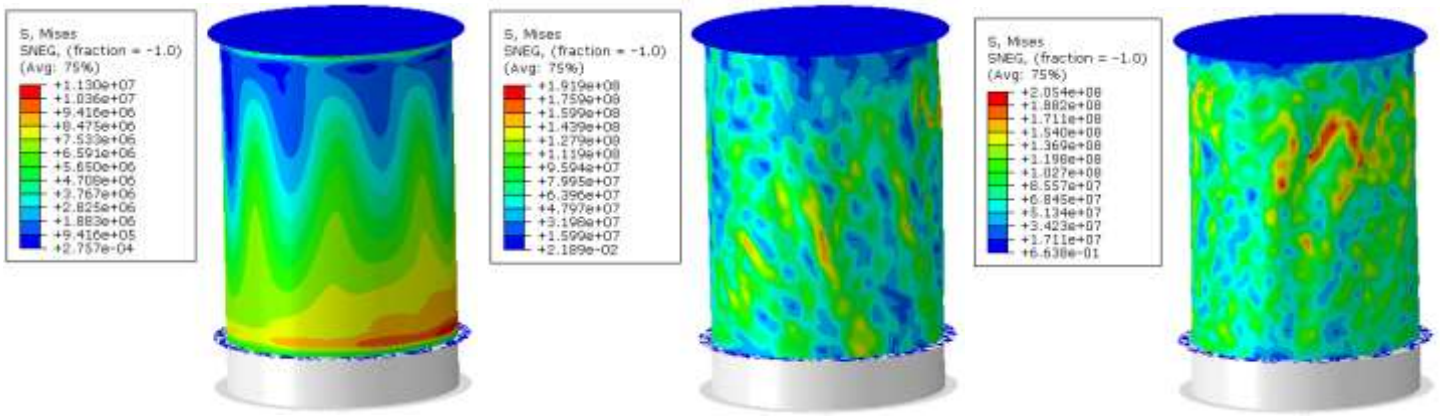

(a). step time = 0.1 sec (b). step time = 0.5 sec (c). step time = 1.0 sec

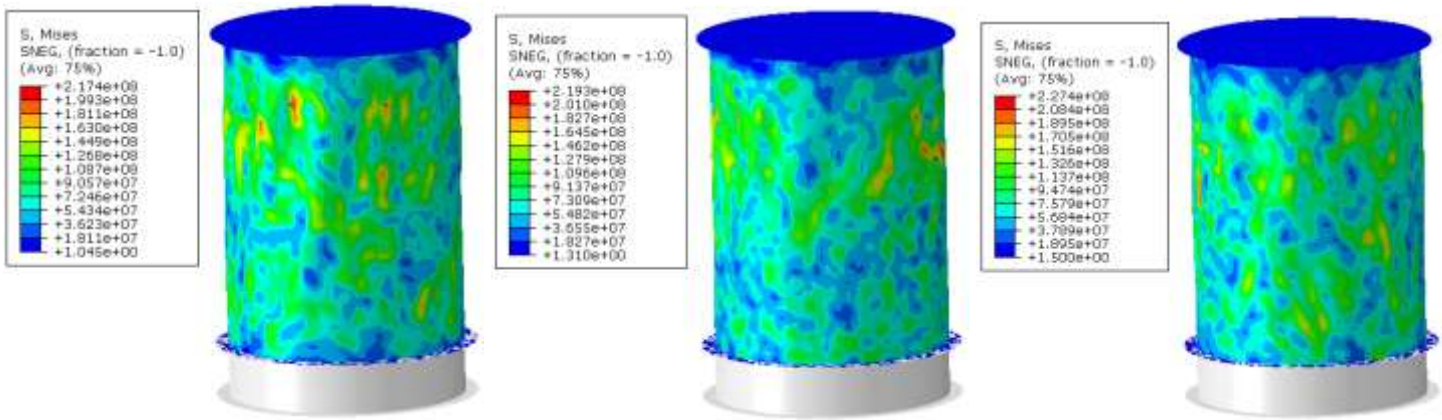

(d). step time = 1.3 sec (e). step time = 2.3 sec (f). step time = 2.4 sec

Figure 8. Von Mises stress distribution at different step time (input excitation = 2.7g)

The dynamic response of the aluminum storage tank was investigated under steady-state sinusoidal excitations with peak excitation amplitudes of 2.7*g*, 3.0*g*, and 3.2*g*, with emphasis on the evolution

of deformation, stress distribution, time history of shear force and bending moment, and hydrodynamic pressure. The deformation contours obtained at different time instants show a clear time-dependent progression of displacement patterns. As illustrated in Fig. 6 (a-f) and Fig. 7 (a-c) for the 2.7*g*, and 3.0*g* excitations, the deformation initially develops in a relatively smooth manner and gradually localizes along the shell wall as the excitation continues.

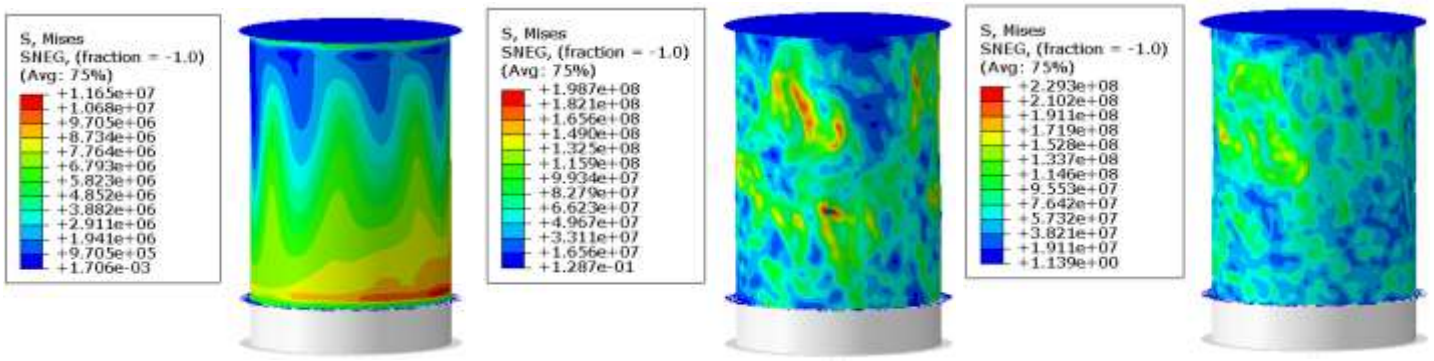

(a). step time = 0.1 sec (b). step time = 0.5 sec (c). step time = 2.7 sec

Figure 9. Von Mises stress distribution at different step times (input excitation = 3.2 *g*)

With increasing excitation level, the overall deformation demand increases, while the spatial characteristics of the deformation pattern remain similar, suggesting a stable deformation mechanism governed by the fluid interaction with the tank wall. Similarly, the corresponding von Mises stress contours, shown in Fig. 8 (a-f) and Fig. 9 (a-c) for excitation levels of 2.7*g* and 3.2*g*, respectively, reveal a progressive redistribution of stresses over time. At early stages, the stress field is relatively uniform and dominated by global membrane action near the tank bottom. As the response evolves, localized stress concentrations emerge and migrate along the shell height, reflecting transient interaction between liquid motion and shell deformation. The peak von Mises stresses were found to be 227.4 MPa, 231.0 MPa, and 229.3 MPa for input excitations of 2.7*g*, 3.0*g*, and 3.2*g*, respectively. Additionally, the maximum hydrodynamic pressure represented by the peak POR values, further reflects the nonlinear nature of the cylindrical storage tank. The

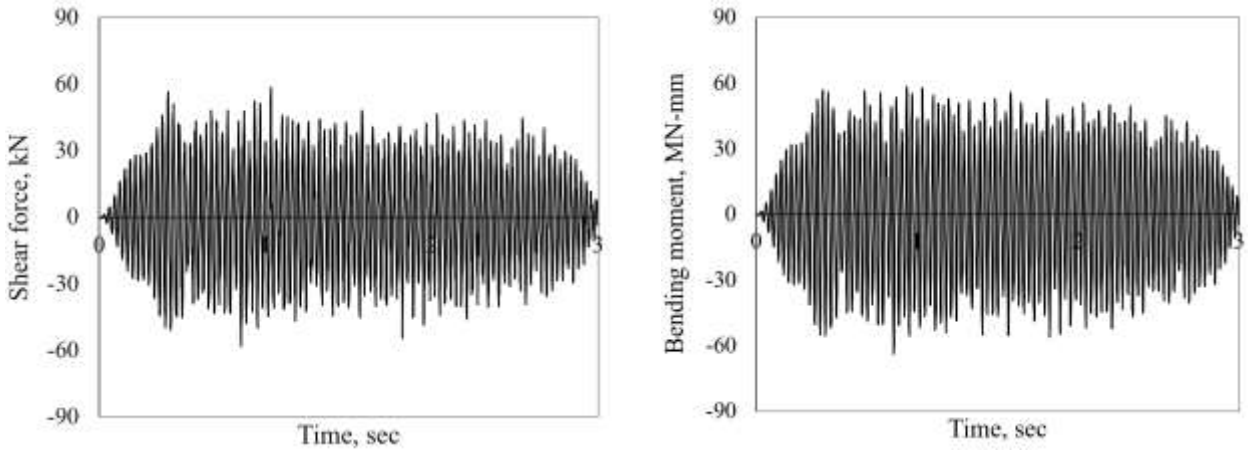

(a) (b)

Figure 10. Time history (a). shear force and (b). bending moment (input excitation = 2.7 *g*)

maximum POR pressures were 463.80 kPa, 446.64 kPa, and 471.20 kPa for excitation levels of 2.7g, 3.0g, and 3.2g, respectively. This behavior can be attributed to nonlinear sloshing dynamics, phase differences between fluid motion and shell response, and redistribution of pressure along

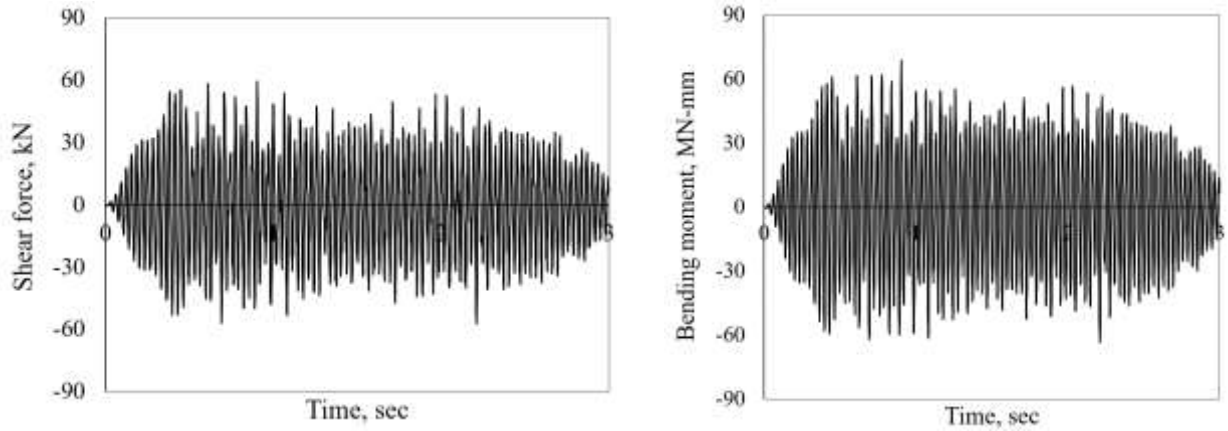

(a) (b)

Figure 11. Time history (a). shear force and (b). bending moment (input excitation = 3.0 *g*)

the tank wall under steady-state excitation. In contrast, the global response quantities show a clearer sensitivity to the input excitation intensity. The base shear increased from 58.53 kN at 2.7*g* to 59.42 kN at 3.0*g* and further to 67.91 kN at 3.2*g*, indicating a substantial amplification at higher excitation levels. A similar trend is observed for the bending moment, which increased from 62.94 MN-mm to 68.74 MN-mm and reached 78.00 MN-mm at the corresponding input excitation of 3.2*g*. The time histories of shear force and bending moment at various input excitation levels are illustrated in Figs. 10-12. These results demonstrate that the shear force and bending demands on the tank increase significantly with stronger excitation.

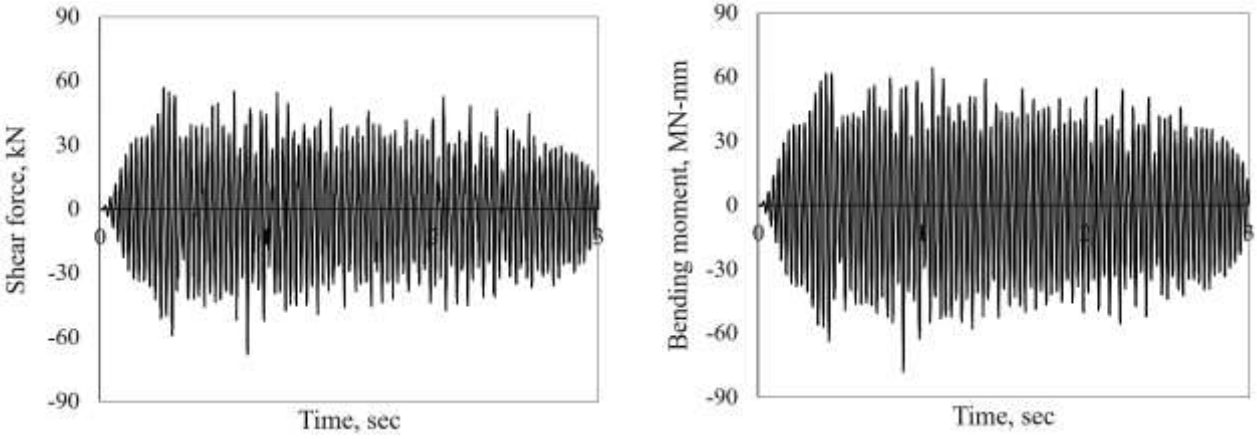

(a) (b)

Figure 12. Time history (a). shear force and (b). bending moment (input excitation = 3.2 *g*)

Overall, the combined results indicate that increasing excitation amplitude leads to a consistent increase in global response measures such as base shear and bending moment, whereas local response quantities, including von Mises stress and hydrodynamic pressure, exhibit non-

monotonic and time-dependent behavior. The deformation and stress contour plots further confirm that the tank response is governed by complex FSI mechanisms and dynamic redistribution effects, underscoring the necessity of high-fidelity nonlinear modeling for accurate assessment of storage tank performance under steady-state dynamic excitations.

4. Conclusions

This study presented a high-fidelity FE investigation of the dynamic response of a cylindrical aluminum storage tank subjected to steady-state sinusoidal excitations with input excitation amplitudes of 2.7g, 3.0g, and 3.2g. The analysis focused on the time evolution of deformation, stress redistribution, global force demands, and hydrodynamic pressure to capture the complex FSI mechanisms governing the tank behavior. First, the accuracy of the FEM is validated through comparison with available experimental results in the literature. The close agreement observed in terms of base shear and bending moment confirms that the FE model can reliably capture the dynamic behavior of storage tanks, including the complex effects of FSI. Key findings from the present study are summarized below.

- The FE model predicts a peak shear force of 44.27 kN, compared with 47.30 kN measured experimentally, yielding a discrepancy of 6.41%. Similarly, the predicted bending moment of 57.90 MN-mm compares well with the experimental value of 61.37 MN-mm, resulting in a difference of 6.19%.

- From the parametric investigation, the results demonstrate both the deformation response and stress concentration is strongly time-dependent.

- The von Mises stress response exhibits a nonlinear trend with increasing the input excitations. Peak stresses of 227.4 MPa, 231.0 MPa, and 229.3 MPa were obtained for excitation levels of 2.7g, 3.0g, and 3.2g, respectively. Stress contours reveal an initial global membrane-dominated response, followed by localized stress redistribution as the dynamic interaction between the liquid and the shell intensifies.

- In contrast, global response measures show a clear sensitivity to excitation intensity. The base shear increased from 58.53 kN at 2.7g to 59.42 kN at 3.0g and reached 67.91 kN at 3.2g, indicating a substantial amplification of inertial forces at higher excitation levels. Similarly, the bending moment increased from 62.94 MN-mm to 68.74 MN-mm and further to 78.00 MN-mm, demonstrating a strong correlation between excitation amplitude and overturning demand.

- The maximum hydrodynamic pressure as represented by peak POR values of 463.80 kPa, 446.64 kPa, and 471.20 kPa under 2.7g, 3.0g, and 3.2g, respectively, does not follow a monotonic trend with increasing excitation. This behavior reflects nonlinear sloshing effects, phase differences between fluid motion and shell response, and pressure redistribution along the tank wall under steady-state excitation.

Future Study/Recommendation

To further advance the understanding of the dynamic behavior of storage tanks involving complex fluid–structure and soil–structure interaction mechanisms, future work will focus on large

cylindrical steel storage tanks with varying liquid fill levels, realistic earthquake ground motions, and the effects of soil–foundation flexibility. Different geometric configurations, including slender and broad tanks, will be investigated under a range of seismic loading scenarios to evaluate their seismic performance. The resulting response measures will be incorporated into fragility-based and performance-based evaluation frameworks to support risk-informed design and assessment of liquid storage tanks.

Acknowledgments
The authors thank the University of North Dakota, Department of Civil Engineering, for providing the commercial software ABAQUS.

References

Bakalis, K., M. Fragiadakis, and D. Vamvatsikos. 2017. "Surrogate Modeling for the Seismic Performance Assessment of Liquid Storage Tanks." *Journal of Structural Engineering*, 143 (4): 04016199. https://doi.org/10.1061/(ASCE)ST.1943-541X.0001667.

Bakalis, K., and S. A. Karamanos. 2021. "Uplift mechanics of unanchored liquid storage tanks subjected to lateral earthquake loading." *Thin-Walled Structures*, 158: 107145. https://doi.org/10.1016/j.tws.2020.107145.

Bektaş, N., and E. Aktaş. 2023. "Seismic Vulnerability Assessment of an Unanchored Circular Storage Tank Against Elephant's Foot Buckling." *Journal of Vibration Engineering & Technologies*, 11 (4): 1661–1678. https://doi.org/10.1007/s42417-022-00663-0.

Buratti, N., and M. Tavano. 2014. "Dynamic buckling and seismic fragility of anchored steel tanks by the added mass method." *Earthquake Engineering & Structural Dynamics*, 43 (1): 1–21. https://doi.org/10.1002/eqe.2326.

Chen, Y., W. Hwang, and C. Ko. 2007. "Sloshing behaviors of rectangular and cylindrical liquid tanks subjected to harmonic and seismic excitations." *Earthquake Engineering & Structural Dynamics*, 36 (12): 1701–1717. https://doi.org/10.1002/eqe.713.

Dhulipala, S. L. N., C. Bolisetti, L. B. Munday, W. M. Hoffman, C. Yu, F. U. H. Mir, F. Kong, A. D. Lindsay, and A. S. Whittaker. 2022. "Development, verification, and validation of comprehensive acoustic fluid-structure interaction capabilities in an open-source computational platform." *Earthquake Engineering & Structural Dynamics*, 51 (10): 2188–2219. https://doi.org/10.1002/eqe.3659.

Jing, W., J. Shen, X. Cheng, and W. Yang. 2022. "Seismic responses of a liquid storage tank considering structure-soil-structure interaction." *Structures*, 45: 2137–2150. https://doi.org/10.1016/j.istruc.2022.10.003.

Lyu, Y., J. Sun, Z. Sun, L. Cui, and Z. Wang. 2020. "Simplified mechanical model for seismic design of horizontal storage tank considering soil-tank-liquid interaction." *Ocean Engineering*, 198: 106953. https://doi.org/10.1016/j.oceaneng.2020.106953.

Maekawa, A. 2012. "Recent Advances in Seismic Response Analysis of Cylindrical Liquid Storage Tanks." *Earthquake-Resistant Structures - Design, Assessment and Rehabilitation*, edited by A. Moustafa. InTech.

Maekawa, A., K. Fujita, and T. Sasaki. 2007. "Dynamic Buckling Test of Modified 1/10 Scale Model of Cylindrical Water Storage Tank." In: *Volume 8: Seismic Engineering*, 311–320. San Antonio, Texas, USA: ASMEDC.

Ozdemir, Z., M. Souli, and Y. M. Fahjan. 2010. "Application of nonlinear fluid–structure interaction methods to seismic analysis of anchored and unanchored tanks." *Engineering Structures*, 32 (2): 409–423. https://doi.org/10.1016/j.engstruct.2009.10.004.

Rammerstorfer, F. G., K. Scharf, and F. D. Fisher. 1990. "Storage Tanks Under Earthquake Loading." *Applied Mechanics Reviews*, 43 (11): 261–282. https://doi.org/10.1115/1.3119154.

Rawat, A., V. Matsagar, and A. K. Nagpal. 2020. "Seismic Analysis of Steel Cylindrical Liquid Storage Tank Using Coupled Acoustic-Structural Finite Element Method for Fluid-Structure Interaction." *The International Journal of Acoustics and Vibration*, 25 (1): 27–40. https://doi.org/10.20855/ijav.2020.25.11499.

Rawat, A., V. Mittal, T. Chakraborty, and V. Matsagar. 2019. "Earthquake induced sloshing and hydrodynamic pressures in rigid liquid storage tanks analyzed by coupled acoustic-structural and Euler-Lagrange methods." *Thin-Walled Structures*, 134: 333–346. https://doi.org/10.1016/j.tws.2018.10.016.

Sobhan, M. S., F. R. Rofooei, and N. K. A. Attari. 2017. "Buckling behavior of the anchored steel tanks under horizontal and vertical ground motions using static pushover and incremental dynamic analyses." *Thin-Walled Structures*, 112: 173–183. https://doi.org/10.1016/j.tws.2016.12.022.

Ullah, S., and I. H. P. Mamaghani. 2025. “Numerical Analysis of Seismic Behavior in Cylindrical Steel Storage Tanks with Liquid Contents Involving Fluid–Structure Interaction.” *Journal of Structural Design and Construction Practice*, 30 (4): 04025095. https://doi.org/10.1061/JSDCCC.SCENG-1770.

Ullah, S., and I. H. P. Mamaghani. 2026. “Seismic Performance Assessment of Cylindrical Liquid-Filled Storage Tanks Considering Fluid–Structure Interaction.” *Journal of Structural Engineering*, 152 (3): 04025286. https://doi.org/10.1061/JSENDH.STENG-15241.

Ulloa-Rojas, J., J. Colombo, J. Wilches, R. León, and J. Almazán. 2024. “Influence of soil - foundation - tank interaction on buckling strength of liquid storage tanks.” *Engineering Structures*, 305: 117744. https://doi.org/10.1016/j.engstruct.2024.117744.

Zhao, Y., Q. Qin, H. Li, and S. Nagarajaiah. 2026. “Numerical simulation analysis of large LNG storage tanks with novel seismic mitigation measures based on fluid-structure interaction.” *Soil Dynamics and Earthquake Engineering*, 201: 109925. https://doi.org/10.1016/j.soildyn.2025.109925.